

# Tuning the stress induced martensitic formation in titanium alloys by alloy design

C. Li · J. H. Chen · X. Wu · W. Wang ·  
S. van der Zwaag

Received: 20 November 2011 / Accepted: 7 January 2012 / Published online: 24 January 2012  
© Springer Science+Business Media, LLC 2012

**Abstract** Two novel titanium alloys, Ti–10V–2Cr–3Al and Ti–10V–1Fe–3Al (wt%), have been designed, fabricated, and tested for their intended stress-induced martensitic (SIM) transformation behavior. The results show that for Ti–10V–1Fe–3Al the triggering stress for SIM transformation is independently affected by the  $\beta$  domain size and  $\beta$  phase stability, when the value of the molybdenum equivalent is higher than  $\sim 9$ . The triggering stress was well predicted using the equations derived separately for the commercial Ti–10V–2Fe–3Al alloy. For samples containing  $\beta$  with a lower molybdenum equivalence value, pre-existing thermal martensite is also present and this was found to have an obstructive effect on SIM transformation. In Ti–10V–2Cr–3Al, the low diffusion speed of Cr caused local gradients in the Cr level for many heat treatments leading even to martensite free zones near former  $\beta$  regions.

## Introduction

Titanium and its alloys start to gain a unique position among other structural materials, like Fe, Al, Ni-based alloy. Titanium alloys are attractive and sometimes indispensable materials from a “materials selection” perspective, due to their very good combination of mechanical and corrosion and erosion resistance [1]. As in other metallic systems showing two stable or meta-stable crystal structures at room temperature, titanium alloys offer many opportunities to tailor the microstructure and the resulting deformation behavior and resulting application fields [2–4].

The importance of metastable  $\beta$  titanium alloy has constantly increased, mainly because the wide range of complex microstructures enable material designers to optimize for both strength and toughness. Phase transformation resulting from the deformation of metals, like steel, are intentionally used to improve properties [5, 6]. It is generally accepted that metastable grades of  $\beta$  titanium alloys may undergo deformation via the formation of SIM [7–18]. Control of this mechanism could provide a new route to the optimization of the load bearing capabilities of titanium alloys. Earlier transformation plasticity studies in titanium alloys like Ti–10V–2Fe–3Al [15, 19],  $\beta$ -Cez [20], and Ti–8.0Mo–3.9Nb–2.0V–3.1Al [21] have shown that the SIM formation starting from a metastable  $\beta$  phase can indeed result in an improved balance of strength and ductility. Studies [7, 22] on SIM confirmed that the martensitic structure is orthorhombic. Our previous work [23] in Ti–10V–2Fe–3Al alloy demonstrated that the triggering stress for SIM is independently affected by the  $\beta$  grain (or domain) size and  $\beta$  phase stability ( $Mo_{eq}$ ). These two factors compete with each other, and eventually decide the triggering stress values. The equation describing the SIM triggering stress as a function of the chemical stability and the grain size of the transforming  $\beta$

---

C. Li (✉) · J. H. Chen  
College of Materials Science and Engineering, Hunan  
University, Changsha, Hunan 410082, China  
e-mail: liconghtu@126.com

C. Li · X. Wu · S. van der Zwaag  
Faculty of Aerospace Engineering, Delft University  
of Technology, Kluyverweg 1, 2629 HS Delft, The Netherlands

X. Wu  
Materials Innovation Institute M2i, Mekelweg 2, 2628 CD Delft,  
The Netherlands

W. Wang  
Institute of Metal Research, Chinese Academy of Sciences,  
Shenyang 110015, China

phase was developed for the Ti–10V–2Fe–3Al alloy but the equation could have a wider application range and be valid for other alloy systems too.

In the present study, two novel alloys with anticipated related tendencies toward SIM formation (Ti–10V–2Cr–3Al and Ti–10V–1Fe–3Al) have been prepared on the basis of the concepts and results of the Ti–10V–2Fe–3Al alloy. The aim of the present study was to make use of those parameters to guide the synthesis of new alloys and to assess the conditions for the occurrence of the expected SIM formation.

## Materials and experiments

Defining new alloy base compositions for tailored SIM behavior

Inspired by the Ti–10V–2Fe–3Al alloy displaying a tunable SIM behavior, new alloy compositions having the potential to optimally exhibit such effect have been designed as follows. The main criteria considered for designing new alloy compositions with a (quantified) stability of in the 100%  $\beta$  state are the martensite start temperature  $M_s$  and the molybdenum equivalency. Both depend on the chemical composition according to Eqs. 1 and 2, respectively [24, 25]

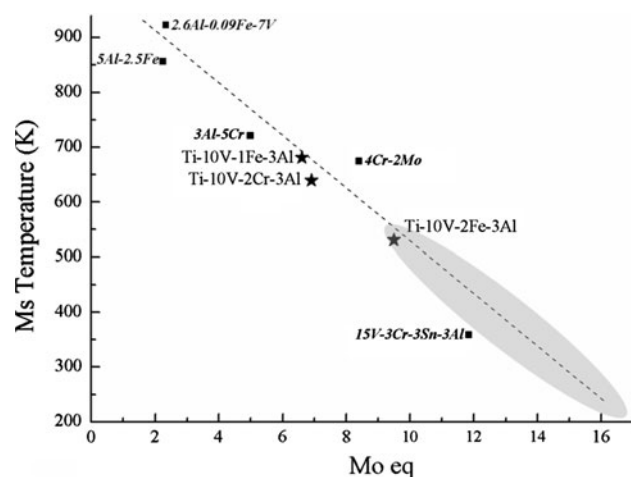


**Fig. 1** Validation of the designed new alloys composition in the  $M_s$  versus Mo eq. map

**Table 1** The achieved compositions (in wt%) of the fabricated new alloys

Ti–10V–2Cr–3Al	V	Cr	Al	O	C	N	H
	10.6	2.18	3.19	0.1	0.05	0.013	0.001
Ti–10V–1Fe–3Al	V	Fe	Al	O	C	N	H
	9.97	0.97	3.02	0.11	0.051	0.014	0.001

$$M_s(K) = 1156 - 150Fe_{wt\%} - 96Cr_{wt\%} - 49Mo_{wt\%} - 37V_{wt\%} - 17Nb_{wt\%} - 7Zr_{wt\%} + 15Al_{wt\%} \quad (1)$$

$$Mo \text{ Eq} = 1.00 Mo_{wt\%} + 0.28Nb_{wt\%} + 0.22Ta_{wt\%} + 0.67V_{wt\%} + 1.6Cr_{wt\%} + 2.9Fe_{wt\%} - 1.00Al_{wt\%} \quad (2)$$

Figure 1 shows the phase stability map calculated for titanium alloys. The reference alloy Ti–10V–2Fe–3Al is situated in the lower right direction relative to the two new alloys, with a relatively lower  $M_s$  temperature and a higher  $Mo_{eq}$  value. This stability value is assumed to apply to both a fully  $\beta$  microstructure and to the  $\beta$  fraction in a mixed  $\alpha$ – $\beta$  microstructure. As the formation of the  $\alpha$  fraction during annealing in the intercritical region induces compositional changes due to alloying element partitioning, the stability of the  $\beta$  fraction increases with the  $\alpha$  fraction formed. For the reference of Ti–10V–2Fe–3Al alloy, SIM behavior was observed for its  $\beta$  fraction under the conditions  $\sim 9 < Mo_{eq} \beta \text{ fraction} < \sim 16$  or  $\sim 550 \text{ K} < M_s < \sim 200 \text{ K}$ . The lower boundary  $Mo_{eq}$  value of  $\sim 9$  (corresponding to the upper boundary for the  $M_s$  temperature) is determined by the chemical composition of the base alloy while the upper  $Mo_{eq}$  boundary value of  $\sim 16$  was determined from the result of an increased (chemical) stability of the  $\beta$  phase as well as an additional stabilizing effect of a smaller  $\beta$  grain size for high  $\alpha$  fractions. The chemical stability aspect has also been explored in [7] by performing deformation studies over a wide temperature range.

In order to get a more accurate and generally defined compositional or compositional/microstructural window for controlled SIM formation, two novel titanium alloys have been designed and prepared with a nominal composition Ti–10V–2Cr–3Al and Ti–10V–1Fe–3Al. Their stability values for the fully  $\beta$  state are also indicated in Fig. 1.

The new alloys Ti–10V–2Cr–3Al and Ti–10V–1Fe–3Al have been fabricated on a laboratory scale by the Institute of Metal Research, Chinese Academy of Science, Shenyang, China. Each alloy weighing about 5 kg was obtained in a forged condition. The  $\beta$  transus temperatures for the materials in its as-received state have been measured using dilatometer. The measured  $\beta$  transus values of Ti–10V–2Cr–3Al alloy and Ti–10V–1Fe–3Al alloy are approximately  $810 \pm 5 \text{ }^\circ\text{C}$  and  $830 \pm 5 \text{ }^\circ\text{C}$ , respectively. The actual compositions are listed in Table 1. The as-received microstructure of the Ti–10V–2Cr–3Al alloy shows a high

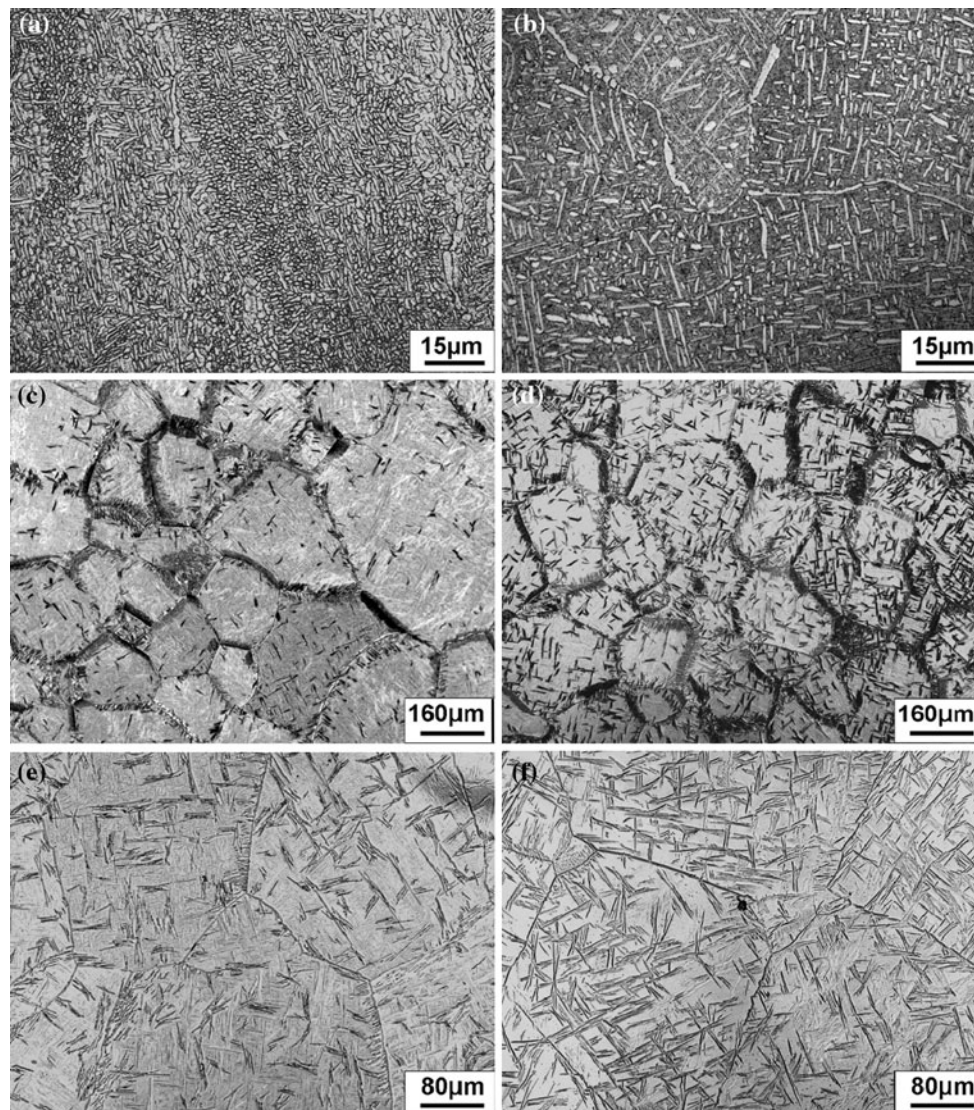


**Fig. 2** Micrographs of different samples: **a** as-received condition of Ti-10V-2Cr-3Al alloy, **b** as-received condition of Ti-10V-1Fe-3Al alloy, **c** 900 °C/15 min + 700 °C/20 min for Ti-10V-2Cr-3Al alloy,

**d** 900 °C/15 min + 700 °C/25 min for Ti-10V-2Cr-3Al alloy, **e** 900 °C/15 min + 750 °C/20 min for Ti-10V-1Fe-3Al alloy, **f** 900 °C/15 min + 750 °C/30 min for Ti-10V-1Fe-3Al alloy

volume fraction of very fine  $\alpha$  phase (Fig. 2a). The Ti-10V-1Fe-3Al alloy shows a lower volume fraction of the  $\alpha$  phase which has a mixed morphology (Fig. 2b).

$\alpha + \beta$  region (700 °C or 750 °C) at the cooling rate of 10 °C/s, then soaked and subsequently gas quenched.

#### Heat-treatment procedures

Different heat-treatment schedules have been imposed to create different  $\alpha$  volume fractions, and hence to create  $\beta$  fractions with different chemical compositions and stabilities. The  $\beta + (\alpha + \beta)$  phase field heat treatments were designed to remove the initial  $\alpha$  particles completely and to create acicular  $\alpha$  instead. Table 2 summarizes the heat-treatment schedules applied to the new alloy samples. In this type of heat treatment, the samples were first solutionized in the  $\beta$  phase field (900 °C for 15 min) and then cooled to the

#### Experimental methods

From the as-received thick slab, cylindrical samples of 4 mm diameter and 7 mm length were machined using electrical discharge machining (EDM). The very thin oxidized outer surface layer was removed by careful mechanical polishing before further experimentation. For microstructure analysis additional electropolishing with a solution of 36 mL perchloric acid, 390 mL methanol, 350 mL ethylene glycol, and 24 mL water was used to avoid any transformation of metastable  $\beta$  phase to martensite during mechanical polishing. Standard Kroll's reagent (3 mL



**Table 2** Heat treatments,  $\alpha$  volume fraction and  $\beta$  domain size of two new alloys

Alloy	Heat-treatment schemes	$\alpha$ volume fraction	$\beta$ domain size
Ti–10V–2Cr–3Al	900 °C/15 min	~0%	~200 $\mu\text{m}$
	900 °C/15 min + 700 °C/5 min	~2%	~195 $\mu\text{m}$
	900 °C/15 min + 700 °C/15 min	~5%	~190 $\mu\text{m}$
	900 °C/15 min + 700 °C/20 min	~15%	~125 $\mu\text{m}$
	900 °C/15 min + 700 °C/25 min	~33%	~75 $\mu\text{m}$
	900 °C/15 min + 700 °C/30 min	~42%	~65 $\mu\text{m}$
	900 °C/15 min + 700 °C/45 min	~57%	~50 $\mu\text{m}$
	900 °C/15 min + 700 °C/60 min	~78%	–
Ti–10V–1Fe–3Al	900 °C/15 min	~0%	~200 $\mu\text{m}$
	900 °C/15 min + 700 °C/5 min	~9%	~185 $\mu\text{m}$
	900 °C/15 min + 750 °C/20 min	~19%	~90 $\mu\text{m}$
	900 °C/15 min + 750 °C/30 min	~42%	~70 $\mu\text{m}$
	900 °C/15 min + 700 °C/15 min	~60%	~30 $\mu\text{m}$
	900 °C/15 min + 700 °C/30 min	~68%	~20 $\mu\text{m}$
	900 °C/15 min + 700 °C/45 min	~74%	–

HF + 6 mL HNO<sub>3</sub> + 100 mL H<sub>2</sub>O) was used for revealing the various phases in Ti–10V–1Fe–3Al alloy, but a modified etchant solution for Ti–10V–2Cr–3Al alloy was employed to reveal the microstructure properly (5 mL HF + 10 mL HNO<sub>3</sub> + 30 mL H<sub>2</sub>O). The cylindrical samples were solution treated at the temperatures and for the times listed using a Bahr 805 horizontal dilatometer at a vacuum level of 10<sup>−5</sup> mbar approximately, which was followed by helium gas quenched to room temperature. A thermocouple was spot welded to the sample in longitudinal surface to record and control the heat-treatment temperature. The tendency to stress-induced martensitic (SIM) formation for the various heat treatments has been assessed by compression testing at room temperature at a strain rate of 10<sup>−3</sup> s<sup>−1</sup> in a Gleeble 1500 thermo-mechanical machine. For each annealing condition, 3 samples were deformed. In order to avoid friction between the anvils and the sample surface, a lubricant (Lubriplate<sup>®</sup>) was used. The morphology and distribution of  $\alpha$  phase along with other microstructure features were determined using a scanning laser confocal microscope Olympus LEXT. The  $\alpha$  volume fractions were determined using quantitative metallographic software. Electron probe micro analysis (EPMA) was performed in a JEOL 8800 M JXA microscope to measure the local concentration variations in the microstructures. The concentration data were obtained using a 15 kV and 50 nA beam.

## Results

### Microstructures after heat-treatment

After the  $\beta$  + ( $\alpha$  +  $\beta$ ) phase field heat treatments, the resulting acicular  $\alpha$  phase was either present as isolated

laths inside the grains or as Widmanstätten laths near prior  $\beta$  grain boundaries. Because the  $\beta$  stability of these two new alloys is significantly lower than that of the reference Ti–10V–2Fe–3Al material, in samples with a relatively low  $\alpha$  volume fraction, a noticeable amount of thermal martensite in the retained  $\beta$  phase was present, as shown in Fig. 2c and e as the dense light gray clusters in the  $\beta$  domain. Longer soaking in the  $\alpha$  +  $\beta$  phase field (Fig. 2d, f) resulted in a higher volume fraction of acicular  $\alpha$  phase upon quenching as compared to a shorter soaking time (Fig. 2c, e). At the same time, with the increase in the  $\alpha$  phase fraction, the retained  $\beta$  phase is gradually stabilized, resulting in  $\beta$  domains free of thermal martensite as can be seen in the micrographs.

### Electron probe micro analysis (EPMA)

According to earlier results [26, 27], the  $\alpha$  phase composition does not vary much with the present heat-treatment conditions in the two phase region. Therefore two typical samples, (one for Ti–10V–2Cr–3Al alloy, another for Ti–10V–1Fe–3Al alloy) were chosen for  $\alpha$  composition analysis with EPMA. EPMA measurements were performed on samples which were heat treated at 900 °C/15 min + 700 °C/30 min for Ti–10V–2Cr–3Al alloy and

**Table 3** Average  $\alpha$  composition measured with EPMA

Alloys	Compositions of $\alpha$ phase		
	V	Cr	Al
Ti–10V–2Cr–3Al	5.93	1.34	3.76
	5.35	0.46	3.51

900 °C/15 min + 750 °C/30 min for Ti–10V–1Fe–3Al alloy. Table 3 lists the concentration of the alloying elements. The results show the expected quantitative evidence of element partitioning in the  $\alpha$  phase, which is poor in vanadium and iron (or chromium) and rich in aluminum.

Compression test

Figure 3 shows selected stress–strain curves for the as-received condition and some heat-treated conditions. Most heat-treated conditions result in a double yield phenomenon which is related to the SIM formation [7, 15, 20]. This is also confirmed by Fig. 4, where the micrograph of Ti–10V–1Fe–3Al alloy (900 °C/15 min + 750 °C/30 min, thermal martensite free) after compression testing is shown. The lower yield stress values of the stress–strain curves, being the start of the SIM transformation, have been determined by the method of tangent intersection, as shown in Fig. 3. In Ti–10V–2Cr–3Al alloy, SIM formation shows a reasonable increase in ductility, while in Ti–10V–1Fe–3Al alloy, samples with SIM transformation have a

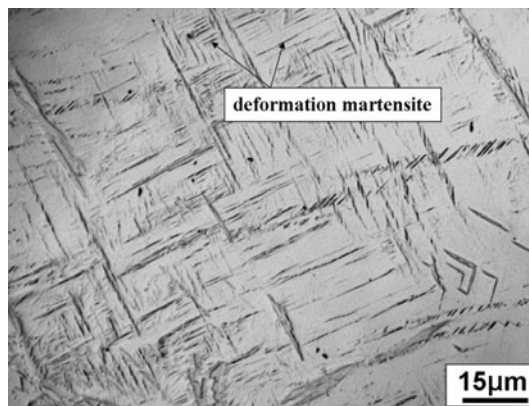


Fig. 4 Typical cross section microstructures of compressed samples: image for Ti–10V–1Fe–3Al alloy (900 °C/15 min + 750 °C/30 min)

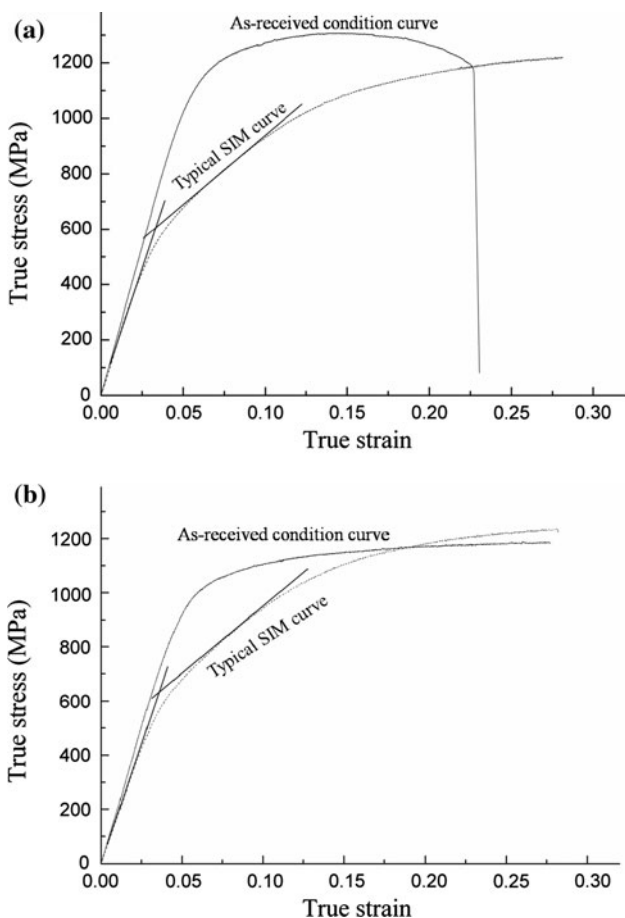


Fig. 3 Compression True stress-true strain curves of different alloys: **a** curves for Ti–10V–2Cr–3Al alloy, **b** curves for Ti–10V–1Fe–3Al alloy

noticeable increase in strength, approximately 10%. The SIM triggering stress as a function of  $\alpha$  volume fraction is shown in Fig. 5. With an increasing  $\alpha$  phase fraction, the stress levels for SIM formation are initially more or less constant, and then increase, as has been observed in the

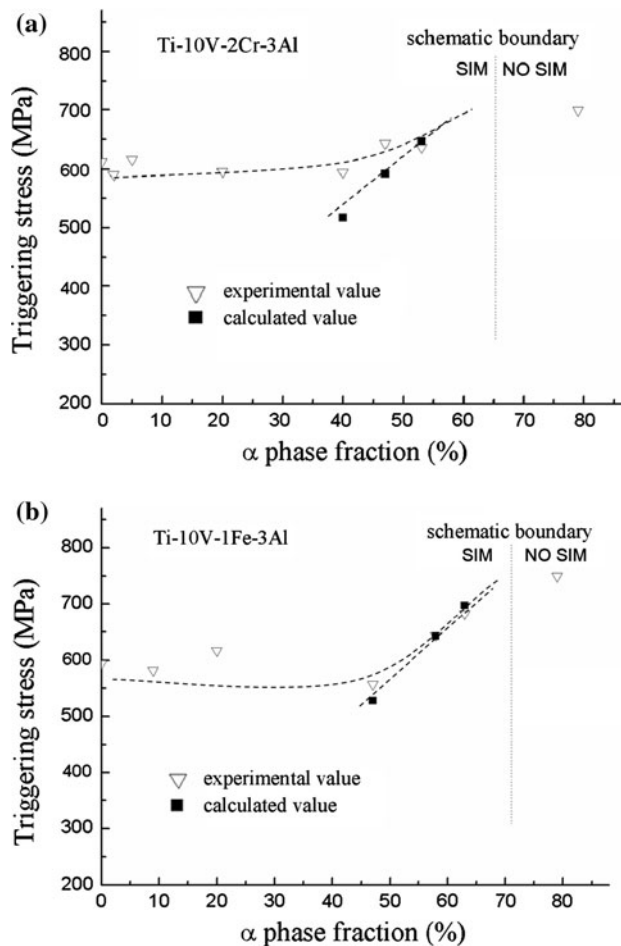


Fig. 5 SIM triggering stress as a function of the  $\alpha$  volume fraction

reference alloy Ti–10V–2Fe–3Al [23]. When the  $\alpha$  phase fraction becomes too high, the SIM formation effect is noted to be absent due to high  $\beta$  stability. The critical  $\alpha$  fractions to block the SIM formation for both alloys are indicated in Fig. 5a and b.

## Discussion

According to our previous research on Ti–10V–2Fe–3Al [23], the triggering stress of SIM formation in this alloy depends on two factors: the chemical stability ( $\text{Mo}_{\text{eq}}$ ) of the  $\beta$  phase and the  $\beta$  grain (or domain) size. A linear superposition of the two effects was found to describe the triggering stress for SIM formation rather well, resulting in the following equation:

$$\sigma_{\text{SIM}}(\text{Mo}_{\text{eq}}, d) = \sigma_{\text{si}}(d)|_{\text{Mo}_{\text{eq}0}} + \Delta\sigma_{\text{st}}(\text{Mo}_{\text{eq}} - \text{Mo}_{\text{eq}0}). \quad (3)$$

where  $\sigma_{\text{SIM}}(\text{Mo}_{\text{eq}}, d)$  is the SIM triggering stress of a metastable  $\beta$  Ti alloy with a specific  $\text{Mo}_{\text{eq}}$   $\beta$  stability and the  $\beta$  domain size  $d$ ;  $\sigma_{\text{si}}(d)|_{\text{Mo}_{\text{eq}0}}$  is the SIM triggering stress for a homogeneous  $\beta$  grain (or domain) of size  $d$  with nominal alloy composition; and  $\Delta\sigma_{\text{st}}(\text{Mo}_{\text{eq}} - \text{Mo}_{\text{eq}0})$  is the change of SIM triggering stress due to the change of chemical composition in the remaining  $\beta$  phase ( $\text{Mo}_{\text{eq}} - \text{Mo}_{\text{eq}0}$ ) as a result of the solute partitioning effect upon  $\alpha$  phase formation, taking a simplified mean field approach to describe the change in  $\beta$  composition. For these two new alloys, the experimental SIM triggering stresses will be analyzed in more detail based on Eq. 3.

It is worth noting that the above quantitative relation between grain size and triggering stress was calculated for Ti–10V–2Fe–3Al, having an initial  $\text{Mo}_{\text{eq}0}$  value of around 9 (based on the actual composition). In order to calculate the  $\beta$  phase  $\text{Mo}_{\text{eq}}$  values for the new alloys as a function of the microstructure resulting from the various heat treatments, the same method as reported in Li et al. [23] was used. By typical  $\alpha$  phase concentrations as measured by EPMA for the new alloys, the resulting mean field  $\beta$  phase concentrations using Eq. 4 can be calculated (taking the density of the  $\alpha$  phase and  $\beta$  phase to be the same).

$$100 \times C_x\% = f_x\% \times C_{x\alpha}\% + (1 - f_x\%) \times C_{x\beta}\% \quad (4)$$

where,  $C_x$  is nominal concentration of  $X$  alloying element (listed in Table 1),  $f_x$  is  $\alpha$  phase volume fraction (listed in Table 2),  $C_{x\alpha}$  is  $X$  alloying element concentration in  $\alpha$  phase (listed in Table 3), and  $C_{x\beta}$  is the resulting  $X$  alloying element concentration in  $\beta$  phase. From this the  $\text{Mo}$  equivalence values for the  $\beta$  fraction can be calculated.

The  $\text{Mo}_{\text{eq}}$  values as a function of the  $\alpha$  volume fraction is now plotted in Fig. 6. When the  $\alpha$  volume fraction increases, the retained  $\beta$  phase becomes more stable, resulting in an increase of the  $\text{Mo}_{\text{eq}}$  value.

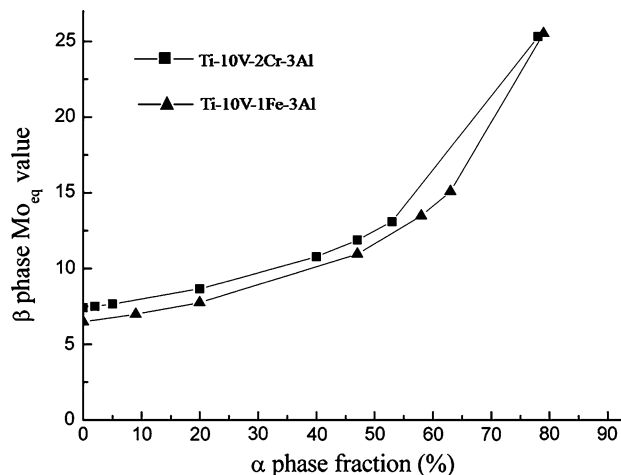
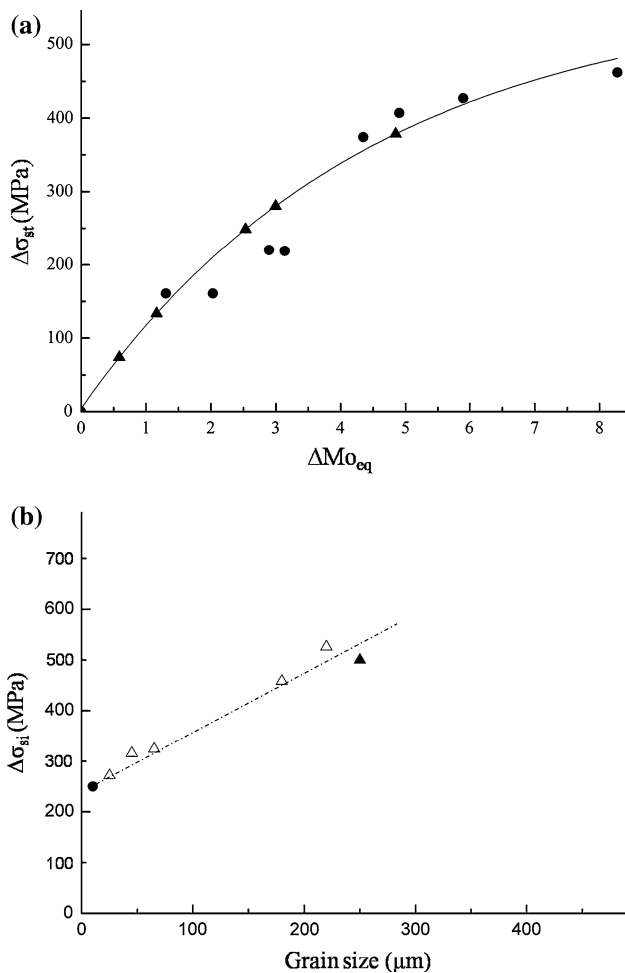


Fig. 6  $\beta$  phase  $\text{Mo}_{\text{eq}}$  value as a function of the  $\alpha$  volume fraction

From the resulting  $\Delta\text{Mo}_{\text{eq}}$  values,  $\Delta\sigma_{\text{st}}$  can be calculated using the curve plotted in Fig. 7a [23]. The size dependent triggering stress component  $\sigma_{\text{si}}(di)|_{\text{Mo}_{\text{eq}0}}$  can be directly obtained from Fig. 7b [23] using the measured  $\beta$  domain sizes in each alloy.

By linear superposition of  $\sigma_{\text{si}}(di)|_{\text{Mo}_{\text{eq}0}}$  and  $\Delta\sigma_{\text{st}}$ , theoretical SIM triggering stress values can be produced which are marked as solid squares in Fig. 5 and are shown together with the experimental values. For Ti–10V–1Fe–3Al alloy, the predicted and the experimental SIM triggering stress are in good agreement for  $\text{Mo}_{\text{eq}} > 9$ . This might be expected for Ti–10V–1Fe–3Al alloy which has the same alloying elements as Ti–10V–2Fe–3Al. The interactions among alloying elements are quite similar between these two alloys, and both alloys should have a similar response to the SIM formation, after taking into account the shift in initial chemical stability due to lowering of the Fe level.

For Ti–10V–2Cr–3Al alloy, deviations are seen between the predicted and experimental values. The predicted values are generally lower than the experimental ones, and this difference becomes greater as  $\text{Mo}_{\text{eq}}$  decreases. The misfit is allocated to the assumed mean field approximation for the composition of the  $\beta$  phase fraction. Compared with iron, chromium has a much lower diffusion coefficient in a titanium matrix [25]. Because of the relatively short solution heat-treatment time in the  $\alpha + \beta$  phase field, most of the Cr atoms cannot diffuse too far away from their original position and they just concentrate near the  $\alpha/\beta$  interphase interface. Therefore,  $\beta$  domains near the interface become very stable, and those areas further away from the interface still have the original stability. Thus, after quenching from a high temperature, such unstable area can still have thermal martensite transformation rather easily.



**Fig. 7** **a** Influence of the  $\beta$  phase stability on triggering stress, **b** triggering stress as a function of the grain size for a fixed  $\beta$  composition of Ti–10V–2Fe–3Al alloy [23]

In order to verify this assumption, a validation experiment was designed and performed. Several cylindrical samples were machined from Ti–10V–2Fe–3Al thick slab, and then heat treated at 900 °C for 60 min followed by 700 °C for 15 min. These heat-treated samples were divided into two groups: samples from group 1 were compressed directly at room temperature in a Gleeble machine i.e., in a condition without thermal martensite. For group 2 samples, the samples were quenched in liquid nitrogen followed by gentle reheating to room temperature before executing the compression test. Mechanical test result shows that samples with thermal martensite (group 2) have significantly higher triggering stress values than samples without thermal martensite being present in the  $\beta$  phase fraction, as clearly shown in Fig. 8.

An additional microstructural feature in the Ti–10V–2Cr–3Al alloy that may alter the generality of the proposed  $\beta$  stability—SIM formation stress relationship is shown in Fig. 9. The feature of martensite free zones near the grain

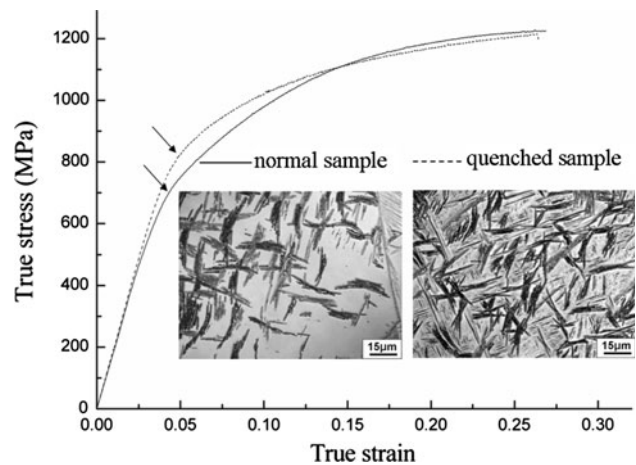


**Fig. 8** Microstructures and compression curves of normal sample and liquid nitrogen quenched sample in Ti–10V–2Fe–3Al

boundaries is quite similar to the “precipitate free zone” observed in precipitation hardenable Al alloys. In the Ti–10V–2Cr–3Al alloy with a low  $\alpha$  fraction, narrow white areas surrounding the acicular  $\alpha$  phase are clearly visible, as indicated in Fig. 9 with arrows. In these white areas, no martensite is formed upon quenching. The possible reason for such a special microstructure, as mentioned before, is the limited diffusion distance of the alloying elements which is affected by the change in  $\alpha$  fraction. For the Ti–10V–1Fe–3Al alloy, the martensite free zone does not form as the redistributed Fe atoms move more quickly and redistribute more or less homogeneously in the residual  $\beta$  phase.

Chen et al. [28] have found the similar microstructures in duplex Fe–Mn–Al–C alloy before. However, until now, no report exists on this kind of “martensite free zone” in titanium alloy. Their influence on mechanical properties needs further investigation.

In order to get a systematic picture of the SIM formation conditions in the three alloys investigated (Ti–10V–2Fe–3Al, Ti–10V–2Cr–3Al, Ti–10V–1Fe–3Al), a schematic map

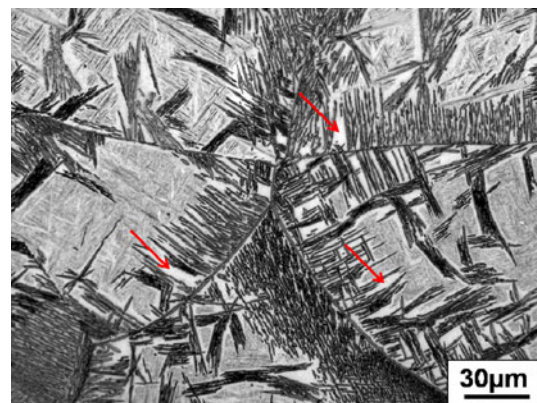


**Fig. 9** “Martensite Free Zone” in Ti–10V–2Cr–3Al alloy, shown with arrows



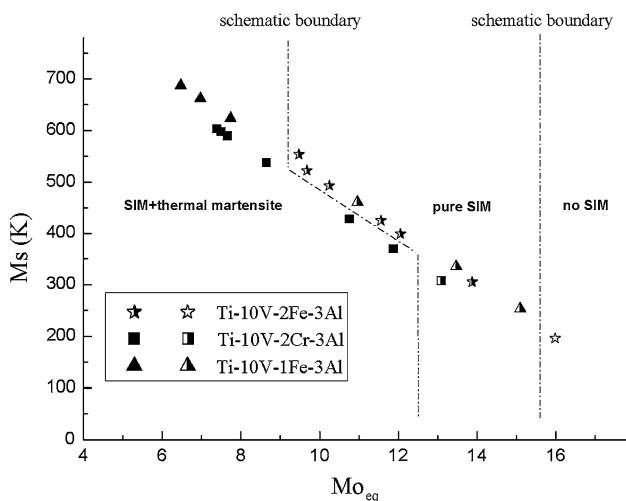


**Fig. 10** SIM transformation comparison for three alloys

of the calculated  $M_s$  temperature of the  $\beta$  phase as a function of  $Mo_{eq}$  value is plotted in Fig. 10. Three characteristic areas can be distinguished: the “thermal martensite + SIM” area, the “pure SIM” area, and the “No SIM” area. Due to their identical alloying element and similar content, boundaries of Ti–10V–2Fe–3Al and Ti–10V–1Fe–3Al almost overlap each other. For Ti–10V–2Cr–3Al, however, because of the lower diffusion coefficient of chromium, the first boundary between thermal martensite + SIM area and pure SIM area shifts significantly.

## Conclusions

The proposed relation between the occurrence of SIM formation upon room temperature compression of metastable titanium alloys derived for Ti–10V–2Fe–3Al was found to apply also to the Ti–10V–1Fe–3Al, albeit that the actual triggering stress was affected by the presence of thermal martensite already present before the compression experiment.

The formation of a “martensite free” zone around the  $\alpha$  phase in the Ti–10V–2Cr–3Al due to a very limited diffusion distance for Cr atoms upon  $\alpha$  formation during intercritical annealing, prevented the wider validation of the proposed relation between the chemical and microstructural  $\beta$  stability.

However, based on the results obtained so far SIM martensite formation is predicted to occur for  $\beta$  phase fractions with  $Mo_{eq}$  value between  $\sim 9$  and  $\sim 16$ . For  $Mo_{eq}$  values lower than  $\sim 9$ , thermal martensite may be present before deformation. For that higher than  $\sim 16$

the  $\beta$  stability is such that even upon deformation the  $\beta$  phase fraction does not transform martensitically.

**Acknowledgements** One of us (X. Wu) acknowledges the financial support by the foundation M2i during the execution of the study. The authors also acknowledge the financial support from the National Basic Research (973) Program of China (No. 2009CB623704) and the Chinese Scholarship Council (CSC).

## References

- Leyens C, Peters M (eds) (2003) Titanium and titanium alloys: fundamentals and applications. Wiley-VCH GmbH & Co, KGaA, Weinheim
- Ganesan P, Gordona S, Deanglis RJ (1980) J Mater Sci 15:1425. doi:10.1007/BF00752122
- Flower HM, Swann PR, West DRF (1972) J Mater Sci 7:929. doi:10.1007/BF00550440
- Fan XG, Yang H, Gao PF (2011) J Mater Sci 46:6018. doi:10.1007/s10853-011-5564-y
- Kundu A, Chakraborti PC (2010) J Mater Sci 45:5482. doi:10.1007/s10853-010-4605-2
- Hufenbach J, Kohlar S, Kuhn U, Giebeler L, Eckert J (2012) J Mater Sci 47:267. doi:10.1007/s10853-011-5794-z
- Neelakantan S (2010) Ph.D. Thesis, Delft University of Technology, Delft
- Kim HS, Lim SH, Yeo ID, Kim WY (2007) Mater Sci Eng A 449:322
- Duerig TW, Terlinde GT, Williams JC (1980) Metall Trans A 11A:1987
- Grosdidier T, Philippe MJ (2000) Mater Sci Eng A 291:218
- Grosdidier T, Roubaud C, Philippe MJ, Zaefferer S, Zandona M, Gautier E, Combres Y (1996) J Phys IV 6:435
- Hideki F (1998) Mater Sci Eng A 243:103
- Ishiyama S, Hanada S, Izumi O (1991) ISIJ Int 31:807
- Mythili R, Paul VT, Saroja S, Vijayalakshmi A, Raghunathan VS (2005) Mater Sci Eng A 390:299
- Neelakantan S, Martin DS, Rivera-Diaz-del-Castillo PEJ, van der Zwaag S (2009) Mater Sci Technol 25:1351
- Wyatt Z, Ankem S (2010) J Mater Sci 45:5022. doi:10.1007/s10853-009-4178-0
- Paradkar A, Kamat SV, Gogia AK, Kashyap BP (2008) Mater Sci Eng A 487:14
- Ouchi C, Fukai H, Hasegawa K (1999) Mater Sci Eng A 263:132
- Sun QY, Song SJ, Zhu RH, Gu HC (2002) J Mater Sci 37:2543. doi:10.1023/A:1015456026919
- Grosdidier T, Combres Y, Gautier E, Philippe MJ (2000) Metall Mater Trans A 31A:1095.
- Zhang LC, Zhou T, Aindow M, Alpay SP, Blackburn MJ (2005) J Mater Sci 40:2833. doi:10.1007/s10853-005-2426-5
- Duerig TW, Albrecht J, Richer D, Fischer P (1982) Acta Metall 30:2161
- Li C, Wu X, Chen JH, van der Zwaag S (2011) Mater Sci Eng A 528:5854
- Neelakantan S, Martin DS, Rivera-Diaz-del-Castillo PEJ, van der Zwaag S (2009) Scripta Mater 60:611
- Lütjering G, Williams JC (2007) Titanium. Springer, Berlin
- Appolaire B, Hericher L, Aebly-Gautier E (2005) Acta Mater 53:3001
- Enomoto M, Yoshida T (1991) ISIJ Int 31:767
- Chen SK, Wan CM, Byrne JG (1990) Mater Res Bull 25:1311